

Weakly nonlinear analysis of a reaction-diffusion model for demyelinating lesions in Multiple Sclerosis

Romina Travaglini^{1,2*}, Rossella Della Marca³

¹INDAM – National Institute for Advanced Mathematics “Francesco Severi”

Piazzale Aldo Moro 5, 00185, Roma, Italy

² Department of Mathematical, Physical and Computer Science, University of Parma

Parco Area delle Scienze 53/A, 43124, Parma, Italy

travaglini@altamatematica.it (*corresponding author)

³Department of Mathematics and Applications “R. Caccioppoli”,

University of Naples “Federico II”,

Via Cintia, Monte S. Angelo I-80126 Napoli, Italy

rossella.dellamarca@unina.it

March 10, 2026

Abstract

Multiple Sclerosis is a chronic autoimmune disorder characterized by the degradation of the myelin sheath in the central nervous system, leading to neurological impairments. In this work, we analyze a reaction-diffusion model derived from kinetic theory to study the formation of demyelinating lesions. We perform a Turing instability analysis and a weakly nonlinear analysis to investigate different spatial patterns that may emerge. Our study examines how key parameters, including the squeezing probability of immune cells and the chemotactic response, impact pattern formation. Numerical simulations confirm the analytical results, revealing the emergence of distinct spatial structures.

1 Introduction

Multiple Sclerosis (MS) is a chronic neurological disorder in which the immune system mistakenly attacks the brain and spinal cord. It is estimated that over 1.8 million people are affected by MS worldwide [43]. The main pathological feature of MS is damage to the myelin sheath, which surrounds axons in the central nervous system and facilitates the transmission of nerve impulses. These lesions can be detected using magnetic resonance

imaging, appearing as focal plaques in the white matter. The symptoms of MS involve a gradual worsening of physical and neurological functions. As the disease progresses, individuals may experience muscle weakness, coordination issues, numbness, vision problems, and cognitive changes. These impairments tend to worsen over time as myelin damage disrupts nerve function. The severity and progression of symptoms can vary between individuals, with some individuals experiencing relapses followed by periods of partial recovery, while others may experience a steady decline. Further details about the clinical overview of MS can be found in [20, 21, 22, 25] and references therein.

The biological mechanisms underlying MS are mainly recognized as those involving immune cells, which are T-cells, B-cells, macrophages, and microglia. These cells can become dysfunctionally activated against myelin-producing cells (oligodendrocytes) or myelin itself, triggering an autoimmune cascade. This inflammatory process is driven by the production of proinflammatory cytokines, molecules produced by immune cells, able to attract themselves and stimulate their clonal expansion.

It is important to note that self-reactive immune cells can also be found in non-pathological conditions [10]. In such cases, the action of specific cells, known as immunosuppressors, can inhibit or eliminate activated immune cells or those cells presenting the antigen able to activate them. What is observed in autoimmune conditions like MS is that the number and effectiveness of these natural killers are compromised [15, 27, 44].

Mathematical modeling represents a powerful framework for understanding the underlying dynamics of MS. On one hand, different models, based on ordinary differential equations [13], stochastic dynamics [6], and systems of partial differential equations (PDE) [3, 4, 7, 18, 23], have been developed to replicate key pathological features. In particular, the systems of PDE proposed have been extensively analyzed using Turing instability and weakly nonlinear analysis. These studies have led to the identification of spatial patterns that mimic myelin lesions typically seen in MS, specifically for type III lesions and Baló's concentric lesions. These lesions are characterized by extensive oligodendrocyte loss, limited T-cell presence, and a lack of remyelination.

On the other hand, the kinetic theory of active particles has been revealed to be effectively applicable to the autoimmune process modeling [11, 19, 8, 12, 26, 24]. This approach has enabled the derivation of macroscopic descriptions of key biological phenomena by starting from the mesoscopic level of cell interactions and cytokine-induced migration [30]. It has been adapted to the specific case of MS [31], offering insights into inflammation, lesion development, and disease progression in the presence of the remyelination process, also including treatment terms [36]. The reaction-diffusion models derived in these works are analyzed through a Turing instability analysis to inquire about pattern formation.

Our present aim is to advance the study of demyelinating lesion formation by performing a weakly nonlinear analysis of a reduced reaction-diffusion system derived from the model introduced in [31], and initially explored in one dimension. In contrast to other models that treat oligodendrocyte loss as an indirect proxy for demyelination [4, 5, 23], the formulation presented in [31] incorporates an explicit state variable representing the fraction of destroyed myelin, enabling a direct and biologically precise description of demyelinating lesions. Although a two-dimensional analysis of a related model was carried

out in [36], that study documented pattern emergence without employing weakly nonlinear techniques. Here, we extend that framework by modeling explicit myelin destruction to two dimensions and applying a weakly nonlinear analysis. Thereby, we establish a novel analytical approach to investigate how key mechanistic parameters—such as squeezing probability and chemotactic sensitivity—govern the spatial organization of demyelinated areas. This methodology captures structured patterns reminiscent of histopathological findings in MS, ranging from elongated plaques [28, 33] to focal or concentric lesions [35, 38]. Consequently, it offers new insights into the emergence of atypical lesion morphologies that cannot be captured in one-dimensional models or in two-dimensional simulations alone without weakly nonlinear analysis.

The chapter is organized as follows: in Section 2, we recall the reaction-diffusion model for MS proposed in [31] and perform a reduction of it. The pattern formation is inquired in Section 3, by performing Turing and weakly nonlinear analysis. Section 4 shows numerical simulations that confirm the results obtained analytically. In Section 5, some concluding remarks are provided.

2 The model

Let us start by recalling the macroscopic reaction-diffusion model derived in [31]. The model describes the formation and restoration of myelin plaques in Multiple Sclerosis and has the following shape:

$$\begin{aligned}
\frac{\partial A(t, \mathbf{x})}{\partial t} &= \alpha + p_{AR} A(t, \mathbf{x}) R(t, \mathbf{x}) - d_{AS} A(t, \mathbf{x}) S(t, \mathbf{x}) - d_A A(t, \mathbf{x}), \\
\frac{\partial S(t, \mathbf{x})}{\partial t} &= p_{SA} S(t, \mathbf{x}) A(t, \mathbf{x}) - d_S S(t, \mathbf{x}), \\
\frac{\partial R(t, \mathbf{x})}{\partial t} &= \nabla_{\mathbf{x}} \cdot [D_R \phi_0(R(t, \mathbf{x})) \nabla_{\mathbf{x}} R(t, \mathbf{x}) - \chi \phi_1(R(t, \mathbf{x})) R(t, \mathbf{x}) \nabla_{\mathbf{x}} C] \\
&\quad + p_{RA} R(t, \mathbf{x}) A(t, \mathbf{x}) - d_{RS} R(t, \mathbf{x}) S(t, \mathbf{x}) - d_R R(t, \mathbf{x}), \\
\frac{\partial C(t, \mathbf{x})}{\partial t} &= D_C \Delta_{\mathbf{x}} C(t, \mathbf{x}) + p_C A(\mathbf{x}, t) R(\mathbf{x}, t) - d_C C(\mathbf{x}, t), \\
\frac{\partial E(t, \mathbf{x})}{\partial t} &= (\bar{E} - E(t, \mathbf{x})) \frac{d_{ER} R(t, \mathbf{x})}{\tilde{r} + R(t, \mathbf{x})} R(t, \mathbf{x}) - r_E E(t, \mathbf{x}).
\end{aligned} \tag{1}$$

The involved quantities are macroscopic densities for: self-antigen presenting cells (A) that can activate the self-reactive immune cells against the myelin; immunosuppressive cells (S) that can inhibit or eliminate activated both self-antigen presenting cells and immune cells; self-reactive immune cells (R); cytokines (C) produced by immune cells when activated by the self-antigen presenting cells; and destroyed fraction of myelin (E). The variables depend on $t \in \mathbb{R}_0^+$ and $\mathbf{x} \in \Gamma_{\mathbf{x}}$, where $\Gamma_{\mathbf{x}}$ is a bounded domain in \mathbb{R}^2 . We underline

that the kinetic description provided in [31] and in the previous works like [12, 24] also include conservative dynamics, whose effects are not observable at the macroscopic level. System (1), indeed, accounts only for the non-conservative processes, which are described below.

The proliferative processes participating in the evolution of A are represented by a constant input source α depending on external factors [34] and proliferative interactions with R . The proliferation of S and R comes from interactions with A , while S destructively interacts with A and R . The production of cytokines comes from the interaction between A and R . Lastly, the consumption of myelin by R is coupled with its restoration by oligodendrocytes, and the last equation in (1) comes from the different time scales considered in [31]. Here, \bar{E} represents the total amount of myelin, which we consider constant in space and time. We also take into account the natural decay of cell populations and cytokines. We take as positive constants all the proliferative and destructive interaction rates, p_{ij} and d_{ij} , respectively, the decay rates d_i , with $i \in \{A, S, R, C, E\}$ and $j \in \{A, S, R\}$, the cytokines production rate p_C , the saturation constant involved in demyelination \tilde{r} , and the remyelination rate r_E .

Moreover, model (1) incorporates: the diffusive dynamics for R , whose coefficient is the constant D_R multiplied by the function ϕ_0 depending on the density; the diffusive dynamics for C , which has a constant diffusion coefficient D_C ; the chemotactic motion of R towards regions where the concentration of cytokines is higher, with a sensitivity function ϕ_1 and the maximal chemotactic rate χ .

The functions ϕ_0 and ϕ_1 are taken as follows [42]

$$\phi_1(y) = \left(1 - \left(\frac{y}{\bar{R}}\right)^\gamma\right) \mathbf{1}_{[0, \bar{R}]}, \quad \phi_0(y) = \phi_1(y) - y \phi_1'(y). \quad (2)$$

The function ϕ_1 is referred to as the *squeezing probability*, i.e., the probability of a cell finding space at its neighboring site. Typically, this probability decreases linearly with the cell density at that site. Here, we consider a rather general form for ϕ_1 by assuming that the *squeezing exponent* γ in (2) can be greater than or equal to one. The term $\mathbf{1}$ is the characteristic function and \bar{R} is the maximal density of self-reactive immune cells. We report in Table 1 all the variables and parameters of model (1)-(2) along with their description.

Table 1: Description of variables and parameters relevant to model (1)–(2).

Symbol	Description
A	Macroscopic density for self-antigen presenting cells
S	Macroscopic density for immunosuppressive cells
R	Macroscopic density for self-reactive immune cells
C	Macroscopic density for cytokines
E	Destroyed fraction of myelin
α	Input source of self-antigen presenting cells
p_{AR}	Proliferative rate of A due to interactions with R

Symbol	Description
p_{SA}	Proliferative rate of S due to interactions with A
p_{RA}	Proliferative rate of R due to interactions with A
p_C	Production rate of cytokines
d_{AS}	Destructive rate of A due to interactions with S
d_{RS}	Destructive rate of R due to interactions with S
d_{ER}	Destructive rate of E due to interactions with R
d_A	Natural decay rate of self-antigen presenting cells
d_S	Natural decay rate of immunosuppressive cells
d_R	Natural decay rate of self-reactive immune cells
d_C	Natural decay rate of cytokines
D_R	Diffusion coefficient for self-reactive immune cells
D_C	Diffusion coefficient for cytokines
χ	Maximal chemotactic rate for self-reactive immune cells
γ	Squeezing exponent
\bar{R}	Maximal density of self-reactive immune cells
\bar{E}	Density of total myelin (both sane and destroyed)
\tilde{r}	Saturation parameter for demyelination
r_E	Remyelination rate

The purpose of the present work is to investigate the formation of lesions in the myelin sheath, caused by the inflammation which is, in turn, induced by the interplay between self-reactive immune cells and cytokines. To this aim, we assume that the populations of self-antigen-presenting cells and immunosuppressive cells are in an equilibrium state, i.e., their temporal derivatives are zero. Consequently, we may derive a reduced form of the system (1), as stated in the following proposition.

Proposition 1. *Let us suppose that the time derivatives of the two populations of self-antigen presenting cells $A(t, \mathbf{x})$ and immunosuppressive cells $S(t, \mathbf{x})$ are zero for all $\mathbf{x} \in \Gamma_{\mathbf{x}}$ and that the two populations are not constantly equal to zero. Then, the system (1) can be reduced to three equations for the quantities $R(t, \mathbf{x})$, $C(t, \mathbf{x})$, and $E(t, \mathbf{x})$, and rewritten in the dimensionless form*

$$\begin{aligned}
\frac{\partial R}{\partial t} &= \nabla_{\mathbf{x}} \cdot (\Phi_0(R) \nabla_{\mathbf{x}} R - \xi \Phi_1(R) \nabla_{\mathbf{x}} C) + R(1 - R), \\
\frac{\partial C}{\partial t} &= \delta \Delta_{\mathbf{x}} C + \beta R - \tau C, \\
\frac{\partial E}{\partial t} &= \frac{\theta R^2}{\Omega + R} (1 - E) - \zeta E.
\end{aligned} \tag{3}$$

Proof. By equalizing to zero the first two equations of system (1), we get

$$A(t, \mathbf{x}) = \frac{d_S}{p_{SA}}, \quad S(t, \mathbf{x}) = \frac{\alpha p_{SA} - d_A d_S}{d_S d_{AS}} + \frac{p_{AR}}{d_{AS}} R(t, \mathbf{x}), \tag{4}$$

by assuming that $S(t, \mathbf{x}) \neq 0$ and $A(t, \mathbf{x}) \neq 0$. We report here that the relations above may be obtained starting from the kinetic description and considering different time scales for the different processes. Nevertheless, we leave this computation for future work. By plugging the expressions (4) into (1), we get

$$\frac{\partial A(t, \mathbf{x})}{\partial t} = 0, \quad (5)$$

$$\frac{\partial S(t, \mathbf{x})}{\partial t} = 0,$$

$$\begin{aligned} \frac{\partial R(t, \mathbf{x})}{\partial t} = & \nabla_{\mathbf{x}} \cdot [D_R \phi_0(R(t, \mathbf{x})) \nabla_{\mathbf{x}} R(t, \mathbf{x}) - \chi \phi_1(R(t, \mathbf{x})) R(t, \mathbf{x}) \nabla_{\mathbf{x}} C] \\ & - d_{RS} R(t, \mathbf{x}) \left(\frac{\alpha p_{SA} - d_A d_S}{d_S d_{AS}} + \frac{p_{AR}}{d_{AS}} R(t, \mathbf{x}) \right) \\ & + R(t, \mathbf{x}) \left(p_{RA} \frac{d_S}{p_{SA}} - d_R \right), \end{aligned}$$

$$\frac{\partial C(t, \mathbf{x})}{\partial t} = D_C \Delta_{\mathbf{x}} C(t, \mathbf{x}) + p_C \frac{d_S}{p_{SA}} R(\mathbf{x}, t) - d_C C(\mathbf{x}, t),$$

$$\frac{\partial E(t, \mathbf{x})}{\partial t} = (\bar{E} - E(t, \mathbf{x})) \frac{d_{ER} R(t, \mathbf{x})}{\tilde{r} + R(t, \mathbf{x})} R(t, \mathbf{x}) - r_E E(t, \mathbf{x}).$$

Thus, defining the coefficients

$$\lambda = \frac{p_{RA} d_S}{p_{SA}} + d_{RS} \frac{d_A d_S - \alpha p_{SA}}{d_S d_{AS}} - d_R, \quad \mu = \frac{p_{AR} d_{RS}}{d_{AS}}, \quad \psi = \frac{p_C d_S}{p_{SA}},$$

we obtain a system of equations, uncoupled from the first two, for the densities R , C , E

$$\begin{aligned} \frac{\partial R(t, \mathbf{x})}{\partial t} = & \nabla_{\mathbf{x}} \cdot [D_R \phi_0(R(t, \mathbf{x})) \nabla_{\mathbf{x}} R(t, \mathbf{x}) - \chi \phi_1(R(t, \mathbf{x})) R(t, \mathbf{x}) \nabla_{\mathbf{x}} C] \\ & + R(t, \mathbf{x}) (\lambda - \mu R(t, \mathbf{x})) \\ \frac{\partial C(t, \mathbf{x})}{\partial t} = & D_C \Delta_{\mathbf{x}} C(t, \mathbf{x}) + \psi R(\mathbf{x}, t) - d_C C(\mathbf{x}, t), \\ \frac{\partial E(t, \mathbf{x})}{\partial t} = & (\bar{E} - E(t, \mathbf{x})) \frac{d_{ER} R(t, \mathbf{x})}{\tilde{r} + R(t, \mathbf{x})} R(t, \mathbf{x}) - r_E E(t, \mathbf{x}). \end{aligned} \quad (6)$$

At this point, we find it convenient to perform the change of variables

$$\tilde{t} = \lambda t, \quad \tilde{\mathbf{x}} = \sqrt{\frac{\lambda}{D_R}} \mathbf{x},$$

in this way, the partial derivatives are

$$\frac{\partial}{\partial t} = \lambda \frac{\partial}{\partial \tilde{t}}, \quad \nabla_{\mathbf{x}} = \sqrt{\frac{\lambda}{D_R}} \nabla_{\tilde{\mathbf{x}}}, \quad \Delta_{\mathbf{x}} = \frac{\lambda}{D_R} \Delta_{\tilde{\mathbf{x}}},$$

so that (6) becomes (omitting the dependence on space and time)

$$\begin{aligned}\frac{\partial R}{\partial \tilde{t}} &= \nabla_{\tilde{\mathbf{x}}} \cdot \left[\phi_0(R) \nabla_{\tilde{\mathbf{x}}} R - \frac{\chi}{D_R} \phi_1(R) R \nabla_{\tilde{\mathbf{x}}} C \right] + R \left(1 - \frac{\mu}{\lambda} R \right), \\ \frac{\partial C}{\partial \tilde{t}} &= \frac{D_C}{D_R} \Delta_{\tilde{\mathbf{x}}} C + \frac{\psi}{\lambda} R - \frac{d_C}{\lambda} C, \\ \frac{\partial E}{\partial \tilde{t}} &= \frac{d_{ER}}{\lambda} (\bar{E} - E) \frac{R^2}{\tilde{r} + R} - \frac{r_E}{\lambda} E,\end{aligned}$$

where we have divided both sides of each equation by λ . The system above can now be written in the dimensionless form by setting

$$\tilde{R} = \frac{\mu}{\lambda} R, \quad \tilde{C} = \frac{\mu d_C}{\lambda \psi} C, \quad \tilde{E} = \frac{E}{\bar{E}},$$

with $\bar{\psi}$ the maximal cytokines production rate for R -cell, providing

$$\begin{aligned}\frac{\partial \tilde{R}}{\partial \tilde{t}} &= \nabla_{\tilde{\mathbf{x}}} \cdot \left[\phi_0 \left(\frac{\lambda}{\mu} \tilde{R} \right) \nabla_{\tilde{\mathbf{x}}} \tilde{R} - \frac{\chi}{D_R} \frac{\psi}{d_C} \phi_1 \left(\frac{\lambda}{\mu} \tilde{R} \right) \tilde{R} \nabla_{\tilde{\mathbf{x}}} \tilde{C} \right] + \tilde{R} (1 - \tilde{R}), \\ \frac{\partial \tilde{C}}{\partial \tilde{t}} &= \frac{D_C}{D_R} \Delta_{\tilde{\mathbf{x}}} \tilde{C} + \frac{\psi d_C}{\bar{\psi} \lambda} \tilde{R} - \frac{d_C}{\lambda} \tilde{C}, \\ \frac{\partial \tilde{E}}{\partial \tilde{t}} &= \frac{d_{ER}}{\mu} (1 - \tilde{E}) \frac{\tilde{R}^2}{\tilde{r} \frac{\mu}{\lambda} + \tilde{R}} - \frac{r_E}{\lambda} \tilde{E}.\end{aligned}$$

We can now define the new coefficients of the model as

$$\begin{aligned}\xi &= \chi \frac{\bar{\psi}}{D_R d_C}, \quad \delta = \frac{D_C}{D_M}, \quad \beta = \frac{\psi d_C}{\bar{\psi} \lambda}, \\ \tau &= \frac{d_C}{\lambda}, \quad \theta = \frac{d_{ER}}{\mu}, \quad \Omega = \frac{\tilde{r} \mu}{\lambda}, \quad \zeta = \frac{r_E}{\lambda},\end{aligned}$$

moreover, we have

$$\phi_1 \left(\frac{\lambda}{\mu} \tilde{R} \right) = \left(1 - \left(\frac{\lambda \tilde{R}}{\mu \bar{R}} \right)^\gamma \right) \mathbf{1}_{U(1-\gamma)},$$

where U is the interval $\{0 \leq \lambda \tilde{R} / \mu \leq \bar{R}\}$, and

$$\phi_0 \left(\frac{\lambda}{\mu} \tilde{R} \right) = \phi_1 \left(\frac{\lambda}{\mu} \tilde{R} \right) - \frac{\lambda \tilde{R}}{\mu} \frac{d \phi_1}{d \tilde{R}} \left(\frac{\lambda}{\mu} \tilde{R} \right) = \phi_1 \left(\frac{\lambda}{\mu} \tilde{R} \right) - \tilde{R} \frac{d \phi_1}{d \tilde{R}} \left(\frac{\lambda}{\mu} \tilde{R} \right).$$

Thus, we introduce the quantity $\mathcal{R} = \mu \bar{R} / \lambda$ and functions

$$\Phi_1(y) = \left(1 - \left(\frac{y}{\mathcal{R}} \right)^\gamma \right) \mathbf{1}_{[0, \mathcal{R}]}(1-\gamma), \quad \Phi_0(y) = \Phi_1(y) - y \Phi_1'(y). \quad (7)$$

At this point, by renaming the non-dimensional variables and densities removing the tilde, we get the system in (3), and this completes the proof.

□

□

3 Pattern formation analysis

In this section, we investigate the properties of the parameters of system (3) to lead to the formation of spatial patterns. To this aim, we add to system (3) the non-negative initial data:

$$\mathbf{W}(0, \mathbf{x}) = \mathbf{W}_0(\mathbf{x}) \geq 0, \text{ with } \mathbf{W} = (R, C, E) \text{ and } R_0 \leq \mathcal{R}, E_0 < 1.$$

We do not consider a maximum level of cytokines, as their production can vary considerably throughout the course of Multiple Sclerosis [1, 17]. We also impose zero-flux conditions at the boundary:

$$(\Phi_0(R) \nabla_{\mathbf{x}} R - \xi \Phi_1(R) R \nabla_{\mathbf{x}} C) \cdot \hat{\mathbf{n}} = 0, \quad \nabla_{\mathbf{x}} C \cdot \hat{\mathbf{n}} = 0, \quad (8)$$

being $\hat{\mathbf{n}}$ the external unit normal to the boundary $\partial\Gamma_{\mathbf{x}}$. We remark that zero-flux boundary conditions are used to prevent external inputs, allowing patterns to emerge intrinsically from the system. This aligns with classical Turing instability results in biological systems [29], where spatial structures arise from internal dynamics rather than boundary effects. From a biological point of view, this is reasonable because, in the brain, the blood–brain barrier effectively isolates the tissue from the external environment. In the context of Multiple Sclerosis, we assume that autoreactive lymphocytes have already infiltrated the central nervous system through the barrier, so the subsequent evolution of demyelinating plaques occurs within this closed environment.

3.1 Turing instability

We want to investigate the capability of the model to describe the formation of plaques in the brain constituted by destroyed myelin. Hence, we perform a Turing instability analysis [37] of system (3) with boundary conditions (8).

The necessary conditions for Turing instability to occur are that the system without spatial gradients has a spatially homogeneous steady state, which turns unstable when adding diffusive and chemotactic terms.

By straightforward computations, we may detect the only nonzero equilibrium of system (3), given by

$$\mathbf{W}_1 = \left(1, \frac{\beta}{\tau}, \frac{\theta}{\theta + \zeta(1 + \Omega)} \right),$$

which is admissible provided that $\mathcal{R} > 1$. By linearizing the system (3) around the equilibrium \mathbf{W}_1 , we have

$$\frac{\partial \mathbf{W}}{\partial t} = \mathbb{D} \Delta_{\mathbf{x}} \mathbf{W} + \mathbb{J} \mathbf{W} \text{ on } (0, \infty) \times \Gamma_{\mathbf{x}}, \quad (9)$$

the diffusion matrix \mathbb{D} and the Jacobian \mathbb{J} write

$$\mathbb{D} = \begin{pmatrix} \tilde{\Phi}_0 & -\xi \tilde{\Phi}_1 & 0 \\ 0 & \delta & 0 \\ 0 & 0 & 0 \end{pmatrix}, \quad \tilde{\Phi}_l = \Phi_l(1), \quad l = 0, 1,$$

and

$$\mathbb{J} = \begin{pmatrix} -1 & 0 & 0 \\ \beta & -\tau & 0 \\ \frac{\zeta \theta (1 + 2\Omega)}{(1 + \Omega)(\zeta + \theta + \zeta \Omega)} & 0 & -\frac{\zeta + \theta + \zeta \Omega}{1 + \Omega} \end{pmatrix},$$

respectively. It is immediate to check that the equilibrium \mathbf{W}_1 is locally asymptotically stable in spatially homogeneous conditions, i.e., when the diffusive and chemotactic processes do not come into play in system (3). Indeed, the characteristic polynomial of the Jacobian is

$$P(\lambda) = -(1 + \lambda)(\lambda + \tau) \left(\lambda + \frac{\zeta + \theta + \zeta \Omega}{1 + \Omega} \right),$$

so that the eigenvalues are $\{-1, -\tau, -(\zeta + \theta + \zeta \Omega)/(1 + \Omega)\}$. Since all eigenvalues have negative real parts, by the standard linearization theory for ordinary differential equations (see, e.g., [2]), the equilibrium \mathbf{W}_1 is asymptotically stable.

Considering the full system (9), we expand the solution in a Fourier series:

$$\mathbf{W}(\mathbf{x}, t) = \sum_k c_k e^{\lambda_k t} \overline{\mathbf{W}}_k(\mathbf{x}), \quad (10)$$

where the eigenfunctions $\overline{\mathbf{W}}_k(\mathbf{x})$ solve the time-independent problem

$$\begin{cases} \Delta_{\mathbf{x}} \overline{\mathbf{W}}_k + k^2 \overline{\mathbf{W}}_k = \mathbf{0}, & \text{on } \Gamma_{\mathbf{x}}, \\ \hat{\mathbf{n}} \cdot \nabla_{\mathbf{x}} \overline{\mathbf{W}}_k = 0, & \text{on } \partial\Gamma_{\mathbf{x}}. \end{cases}$$

Substituting (10) into (9) shows that, for each wavenumber k , the growth rate λ_k is an eigenvalue of the matrix

$$\mathbb{J} - k^2 \mathbb{D}.$$

Thus, instability occurs if there exists a range of wavenumbers $[k_1, k_2]$ such that $\text{Re}(\lambda_k) > 0$ for $k \in [k_1, k_2]$. For our system, the eigenvalues of $\mathbb{J} - k^2 \mathbb{D}$ are

$$\begin{aligned} \lambda_k^0 &= -\frac{\zeta + \theta + \zeta \Omega}{1 + \Omega}, \\ \lambda_k^{\pm} &= \frac{1}{2} \left(-1 - \tau - k^2(\delta + \tilde{\Phi}_0) \pm \sqrt{\left(-1 - \tau - k^2(\delta + \tilde{\Phi}_0) \right)^2 - 4h(k^2)} \right), \end{aligned}$$

where

$$h(k^2) = -\frac{(1 + \Omega) \text{Det}(\mathbb{J} - k^2 \mathbb{D})}{\zeta + \theta + \zeta \Omega} = k^4 \delta \tilde{\Phi}_0 + k^2 \Lambda + \tau, \quad \Lambda = \delta + \tau \tilde{\Phi}_0 - \beta \xi \tilde{\Phi}_1.$$

Since $\lambda_k^0 < 0$, instability can only arise from λ_k^\pm . This requires $h(k^2) < 0$ for some k^2 and corresponds to imposing

$$\Lambda < 0 \quad \text{and} \quad \Lambda^2 - 4\delta\tilde{\Phi}_0\tau > 0.$$

The first condition gives $\xi > (\delta + \tau\tilde{\Phi}_0)/(\beta\tilde{\Phi}_1)$, while the second condition leads to two possibilities:

$$\xi < \frac{\delta + \tau\tilde{\Phi}_0 - 2\sqrt{\delta\tau\tilde{\Phi}_0}}{\beta\tilde{\Phi}_1} \quad \text{or} \quad \xi > \frac{\delta + \tau\tilde{\Phi}_0 + 2\sqrt{\delta\tau\tilde{\Phi}_0}}{\beta\tilde{\Phi}_1}.$$

This leads to the Turing instability condition

$$\xi > \xi_c := \frac{\delta + \tau\tilde{\Phi}_0 + 2\sqrt{\delta\tau\tilde{\Phi}_0}}{\beta\tilde{\Phi}_1}. \quad (11)$$

The corresponding critical wavenumber such that $h(k^2) = 0$ is

$$k_c^2 = \frac{\sqrt{\Lambda^2 - 4\delta\tau\tilde{\Phi}_0} - \Lambda_c}{2\delta\tilde{\Phi}_0} = \sqrt{\frac{\tau}{\delta\tilde{\Phi}_0}}, \quad \text{where } \Lambda_c = \delta + \tau\tilde{\Phi}_0 - \beta\xi_c\tilde{\Phi}_1. \quad (12)$$

3.2 Weakly nonlinear analysis

Once the conditions on parameters leading to the formation of spatial patterns are outlined, we want to reproduce a richer scenario beyond what Turing analysis alone can achieve. Specifically, we perform a two-dimensional weakly nonlinear analysis of the problem, that relies on the fact that, when the control parameter ξ approaches its critical threshold, the system's dynamics evolve more slowly. This property makes it possible to study pattern formation through the use of amplitude equations.

More precisely, as discussed for instance in [40], each possible steady-state configuration of the reaction–diffusion system corresponds to a planform defined by m pairs of wave vectors $(\mathbf{k}_j, -\mathbf{k}_j)$. For critical modes, those satisfying $|\mathbf{k}_j| = k_c$, the solution can be written as

$$\tilde{\mathbf{U}} = \sum_{j=1}^m [\mathbf{A}_j(t) e^{i\mathbf{k}_j \cdot \mathbf{x}} + \bar{\mathbf{A}}_j(t) e^{-i\mathbf{k}_j \cdot \mathbf{x}}], \quad (13)$$

where \mathbf{A}_j denotes the complex amplitude vector associated with the mode \mathbf{k}_j , and $\bar{\mathbf{A}}_j$ is its complex conjugate. Depending on the value of m and the geometric relations among the wave vectors, different pattern symmetries can be investigated. In this work, we focus on the case $m = 2$.

Our aim is, then, to recover an analytical shape for the amplitudes \mathbf{A}_j when the system evolves from a perturbation of the equilibrium state, thus, we start by performing a Taylor expansion of system (3) up to the third order around the equilibrium \mathbf{W}_1 , getting

$$\frac{\partial \mathbf{U}}{\partial t} = \mathcal{L} \mathbf{U} + \mathcal{H}[\mathbf{U}] + O(\mathbf{U}^3), \quad \text{for} \quad \mathbf{U} = \begin{pmatrix} u \\ v \\ w \end{pmatrix} = \mathbf{W} - \mathbf{W}_1, \quad (14)$$

where $\mathcal{L} = \mathbb{D}\Delta_{\mathbf{x}} + \mathbb{J}$ and $\mathcal{H}[\mathbf{U}]$ is

$$\begin{pmatrix} -u^2 + \left(\tilde{\Phi}'_0 + \frac{1}{2} \tilde{\Phi}''_0 u \right) u \Delta_{\mathbf{x}} u + \left(\tilde{\Phi}'_0 + \tilde{\Phi}''_0 u \right) \|\nabla_{\mathbf{x}} u\|^2 + \\ -\xi \left[\left(\tilde{\Phi}'_1 + \frac{1}{2} \tilde{\Phi}''_1 u \right) u \Delta_{\mathbf{x}} v + \left(\tilde{\Phi}'_1 + \tilde{\Phi}''_1 u \right) \nabla_{\mathbf{x}} u \cdot \nabla_{\mathbf{x}} v \right] \\ 0 \\ \frac{\theta}{(1+\Omega)^2} \left(\frac{2u^2 \zeta \Omega^2}{\theta + \zeta(1+\Omega)} - u w (1+2\Omega) + \right. \\ \left. - \frac{u^3 \zeta \Omega^2}{(1+\Omega)(\theta + \zeta(1+\Omega))} - \frac{u^2 w \Omega^2}{1+\Omega} \right) \end{pmatrix},$$

where $\tilde{\Phi}'_l = \Phi'_l(1)$, $\tilde{\Phi}''_l = \Phi''_l(1)$, $l = 0, 1$.

As mentioned before, we can gather information on the formation and shape of patterns when the parameter ξ is close to the critical threshold ξ_c given in (11), thus we expand it in terms of a small parameter η as follows

$$\xi = \xi_c + \eta \xi_1 + \eta^2 \xi_2 + \eta^3 \xi_3 + O(\eta^3). \quad (15)$$

Similarly, the solution vector \mathbf{U} can be expanded as

$$\mathbf{U} = \eta \begin{pmatrix} u_1 \\ v_1 \\ w_1 \end{pmatrix} + \eta^2 \begin{pmatrix} u_2 \\ v_2 \\ w_2 \end{pmatrix} + \eta^3 \begin{pmatrix} u_3 \\ v_3 \\ w_3 \end{pmatrix} + O(\eta^3). \quad (16)$$

When the bifurcation parameter approaches the threshold, the pattern's amplitude changes slowly over time, since the leading term of the nonlinear expansion of the solution is the product of the basic pattern and a slowly varying amplitude [16, 39]. This enables a distinction between fast and slow temporal dynamics, allowing us to introduce multiple time scales as follows:

$$\frac{\partial}{\partial t} = \eta \frac{\partial}{\partial T_1} + \eta^2 \frac{\partial}{\partial T_2} + O(\eta^2). \quad (17)$$

We can now substitute the expansions (16)-(17) in (14), and collecting the terms in the same order of η on each side, we obtain three equations, one for each order:

- order η :

$$\mathcal{L}_c \begin{pmatrix} u_1 \\ v_1 \\ w_1 \end{pmatrix} = 0 \quad \text{with } \mathcal{L}_c = \mathbb{D}_c \Delta_{\mathbf{x}} + \mathbb{J}, \quad \mathbb{D}_c = \begin{pmatrix} \tilde{\Phi}'_0 & -\xi_c \tilde{\Phi}'_1 & 0 \\ 0 & \delta & 0 \\ 0 & 0 & 0 \end{pmatrix} \quad (18)$$

- order η^2 :

$$\frac{\partial}{\partial T_1} \begin{pmatrix} u_1 \\ v_1 \\ w_1 \end{pmatrix} = \mathcal{L}_c \begin{pmatrix} u_2 \\ v_2 \\ w_2 \end{pmatrix} + \mathcal{H}_2 \left[\begin{pmatrix} u_1 \\ v_1 \\ w_1 \end{pmatrix} \right] \quad (19)$$

with

$$\mathcal{H}_2 \left[\begin{pmatrix} u_1 \\ v_1 \\ w_1 \end{pmatrix} \right] = \begin{pmatrix} \tilde{\Phi}'_0 \nabla_{\mathbf{x}} \cdot (u_1 \nabla_{\mathbf{x}} u_1) - \xi_c \tilde{\Phi}'_1 \nabla_{\mathbf{x}} \cdot (u_1 \nabla_{\mathbf{x}} v_1) - \xi_1 d_{12} \Delta_{\mathbf{x}} v_1 - u_1^2 \\ 0 \\ \frac{\theta}{(1+\Omega)^2} \left(\frac{2u_1^2 \zeta \Omega^2}{\theta + \zeta (1+\Omega)} - u_1 w_1 (1+2\Omega) \right) \end{pmatrix}$$

- order η^3 :

$$\frac{\partial}{\partial T_1} \begin{pmatrix} u_2 \\ v_2 \\ w_2 \end{pmatrix} + \frac{\partial}{\partial T_2} \begin{pmatrix} u_1 \\ v_1 \\ w_1 \end{pmatrix} = \mathcal{L}_c \begin{pmatrix} u_3 \\ v_3 \\ w_3 \end{pmatrix} + \mathcal{H}_3 \left[\begin{pmatrix} u_1 \\ v_1 \\ w_1 \end{pmatrix}, \begin{pmatrix} u_2 \\ v_2 \\ w_2 \end{pmatrix} \right] \quad (20)$$

with

$$\mathcal{H}_3 \left[\begin{pmatrix} u_1 \\ v_1 \\ w_1 \end{pmatrix}, \begin{pmatrix} u_2 \\ v_2 \\ w_2 \end{pmatrix} \right] = \begin{pmatrix} \tilde{\Phi}'_0 \nabla_{\mathbf{x}} \cdot (u_1 \nabla_{\mathbf{x}} u_2 + u_2 \nabla_{\mathbf{x}} u_1) + \\ -\xi_c \left[\tilde{\Phi}'_1 \nabla_{\mathbf{x}} \cdot (u_1 \nabla_{\mathbf{x}} v_2 + u_2 \nabla_{\mathbf{x}} v_1) + \frac{1}{2} \tilde{\Phi}''_1 \nabla_{\mathbf{x}} \cdot (u_1^2 \nabla_{\mathbf{x}} v_1) \right] + \\ + \frac{1}{2} \tilde{\Phi}''_0 \nabla_{\mathbf{x}} \cdot (u_1^2 \nabla_{\mathbf{x}} u_1) - \xi_1 \tilde{\Phi}'_1 \nabla_{\mathbf{x}} \cdot (u_1 \nabla_{\mathbf{x}} v_1) + \\ -\xi_1 d_{12} \Delta_{\mathbf{x}} v_2 - \xi_2 d_{12} \Delta_{\mathbf{x}} v_1 - u_1 u_2 \\ 0 \\ \frac{\theta}{(1+\Omega)^2} \left(\frac{4u_1 u_2 \zeta \Omega^2}{\theta + \zeta (1+\Omega)} + \right. \\ \left. - (u_1 w_2 + u_2 w_1) (1+2\Omega) - \frac{u_1^3 \zeta \Omega^2}{(1+\Omega)(\theta + \zeta (1+\Omega))} - \frac{u_1^2 w_1 \Omega^2}{1+\Omega} \right) \end{pmatrix}.$$

Each one of the equalities above can provide information on the corresponding term of the expansion (21) or its time derivative. We start from the equation of order η and claim the following result.

Proposition 2. *The solution of (18) can be expressed as*

$$\begin{pmatrix} u_1 \\ v_1 \\ w_1 \end{pmatrix} = \begin{pmatrix} \rho_R \\ 1 \\ \rho_E \end{pmatrix} \sum_{j=1}^2 [\mathcal{W}_j(t) e^{i \mathbf{k}_j \cdot \mathbf{x}} + \overline{\mathcal{W}_j(t)} e^{-i \mathbf{k}_j \cdot \mathbf{x}}], \quad (21)$$

where $\overline{\mathcal{W}}_j$ is the complex conjugate,

$$\rho_R = \frac{\sqrt{\tau}}{\beta} \left(\sqrt{\tau} + \sqrt{\frac{\delta}{\tilde{\Phi}_0}} \right), \quad (22)$$

and

$$\rho_E = \frac{\zeta \theta \sqrt{\tau} (1 + 2\Omega)}{\beta (\theta + \zeta (1 + \Omega))^2} \left(\sqrt{\tau} + \sqrt{\frac{\delta}{\tilde{\Phi}_0}} \right). \quad (23)$$

Proof. See Appendix A.1.

Successively, we look at the equation of order η^2 , i.e. (19). We can provide the following result.

Proposition 3. *Let us consider the equation (19) and let the vector $(u_1, v_1, w_1)^T$ be in the form (21); then, the equation (19) can be solved if and only if the conditions*

$$(\rho_R + \sigma_C) \frac{\partial \mathcal{W}_j}{\partial T_1} = \xi_1 k_c^2 \tilde{\Phi}_1 \mathcal{W}_j, \quad j = 1, 2, \quad (24)$$

hold, and the solution has the form

$$\begin{aligned} \begin{pmatrix} u_2 \\ v_2 \\ w_2 \end{pmatrix} &= \begin{pmatrix} X_0 \\ Y_0 \\ Z_0 \end{pmatrix} (|\mathcal{W}_1|^2 + |\mathcal{W}_2|^2) + \sum_{j=1}^2 \begin{pmatrix} \rho_R \\ 1 \\ \rho_E \end{pmatrix} \mathcal{V}_j e^{i\mathbf{k}_j \cdot \mathbf{x}} \\ &+ \begin{pmatrix} X_1 \\ Y_1 \\ Z_1 \end{pmatrix} [\mathcal{W}_1 \mathcal{W}_2 e^{i(\mathbf{k}_1 + \mathbf{k}_2) \cdot \mathbf{x}} + \mathcal{W}_1 \overline{\mathcal{W}}_2 e^{i(\mathbf{k}_1 - \mathbf{k}_2) \cdot \mathbf{x}}] \\ &+ \sum_{j=1}^2 \begin{pmatrix} X_2 \\ Y_2 \\ Z_2 \end{pmatrix} \mathcal{W}_j^2 e^{2i\mathbf{k}_j \cdot \mathbf{x}} + c.c., \end{aligned} \quad (25)$$

where *c.c.* indicates the complex conjugate, and being the coefficients X_m, Y_m, Z_m , $m = 0, 1, 2$, given by

$$\begin{pmatrix} X_0 \\ Y_0 \\ Z_0 \end{pmatrix} = -2\rho_R^2 \begin{pmatrix} 1 \\ \beta \\ \tau \\ \Xi_0 \end{pmatrix}, \quad (26)$$

$$\begin{pmatrix} X_1 \\ Y_1 \\ Z_1 \end{pmatrix} = \frac{\rho_R \left(\rho_R + k_c^2 \left(\rho_R \tilde{\Phi}'_0 - \xi_c \tilde{\Phi}'_1 \right) \right)}{1 + 2k_c^2 \tilde{\Phi}_0} \begin{pmatrix} -2 \\ \beta \\ \frac{\beta}{k_c^2 \xi_c \tilde{\Phi}_1} \\ \Xi_1 \end{pmatrix}, \quad (27)$$

$$\begin{pmatrix} X_2 \\ Y_2 \\ Z_2 \end{pmatrix} = \frac{-\rho_R \left(\rho_R + 2k_c^2 \left(\rho_R \tilde{\Phi}'_0 - \xi_c \tilde{\Phi}'_1 \right) \right)}{\tau + 4k_c^2 \left(\delta + \tilde{\Phi}_0 (4k_c^2 \delta + \tau) - \beta \xi_c \tilde{\Phi}_1 \right)} \begin{pmatrix} 4k_c^2 \delta + \tau \\ \beta \\ \Xi_2 \end{pmatrix}, \quad (28)$$

with Ξ_0 , Ξ_1 and Ξ_2 provided in A.2.

Proof. See Appendix A.2.

For what concerns the equation (20) of order η^3 , it leads to the following result.

Proposition 4. *Let us consider the equation (20) and let the vectors $(u_1, v_1, w_1)^T$, $(u_2, v_2, w_2)^T$, be in the form (21) and (25), respectively; then, the equation (20) can be solved if and only if the conditions below are satisfied.*

$$(\rho_R + \sigma_C) \left(\frac{\partial \mathcal{V}_j}{\partial T_1} + \frac{\partial \mathcal{W}_j}{\partial T_2} \right) = k_c^2 \tilde{\Phi}_1 (\xi_2 \mathcal{W}_j + \xi_1 \mathcal{V}_j) + (r_1 |\mathcal{W}_j|^2 + r_2 |\mathcal{W}_l|^2) \mathcal{W}_j, \quad (29)$$

for $j, l = 1, 2$, $j \neq l$, with coefficients

$$\begin{aligned} r_1 &= - (X_0 + X_2) \rho_R \left(2 + k_c^2 \tilde{\Phi}'_0 \right) \\ &\quad + k_c^2 (X_0 - X_2) \xi_c \tilde{\Phi}'_1 + \frac{1}{2} k_c^2 \rho_R \left(\xi_c \left(4Y_2 \tilde{\Phi}'_1 + \rho_R \tilde{\Phi}''_1 \right) - \rho_R^2 \tilde{\Phi}''_0 \right), \\ r_2 &= - (2X_1 + X_0) \rho_R \left(2 + k_c^2 \tilde{\Phi}'_0 \right) + k_c^2 \xi_c (X_0 + 2X_1 \rho_R) \tilde{\Phi}'_1 \\ &\quad - k_c^2 \rho_R^2 \left(\rho_R \tilde{\Phi}_{0s} - \xi_c \tilde{\Phi}_{1s} \right). \end{aligned} \quad (30)$$

Proof. See Appendix A.3.

Now, we look at the expansion (16) and, keeping in mind the expressions (21) and (25), we may assert that the emerging solution given in (13) (with $m = 2$) can be recovered by defining the amplitudes of patterns associated with modes \mathbf{k}_j as

$$\mathbf{A}_j = \eta \begin{pmatrix} \rho_R \\ 1 \\ \rho_E \end{pmatrix} \mathcal{W}_j + \eta^2 \begin{pmatrix} \rho_R \\ 1 \\ \rho_E \end{pmatrix} \mathcal{V}_j + O(\eta^3), \quad j = 1, 2, \quad (31)$$

and their evolution in time, considering the expansion (17), is given by

$$\frac{d\mathbf{A}_j}{dt} = \eta^2 \begin{pmatrix} \rho_R \\ 1 \\ \rho_E \end{pmatrix} \frac{\partial \mathcal{W}_j}{\partial T_1} + \eta^3 \begin{pmatrix} \rho_R \\ 1 \\ \rho_E \end{pmatrix} \left(\frac{\partial \mathcal{W}_j}{\partial T_2} + \frac{\partial \mathcal{V}_j}{\partial T_1} \right) + O(\eta^4), \quad j = 1, 2, \quad (32)$$

We also find it convenient to write amplitudes as $\mathbf{A}_j = (\rho_R A_j, A_j, \rho_E A_j)^T$. At this point, we outline the result for the evolution in time of amplitudes.

Proposition 5. *Let us decompose each $A_j(t)$ into its mode and phase angle as $A_j(t) = \rho_j(t) e^{i\phi_j(t)}$, for $j = 1, 2$. Then, ϕ_1 and ϕ_2 are constant and the evolution in time of ρ_1, ρ_2 is prescribed by the system*

$$\begin{aligned} s_0 \frac{d\rho_1}{dt} &= \xi_m \rho_1 + s_1 \rho_1^3 + s_2 \rho_2^2 \rho_1 \\ s_0 \frac{d\rho_2}{dt} &= \xi_m \rho_2 + s_1 \rho_2^3 + s_2 \rho_1^2 \rho_2, \end{aligned} \quad (33)$$

where

$$s_0 = \frac{\rho_R + \sigma_C}{k_c^2 \xi_c \tilde{\Phi}_1}, \quad \xi_m = \frac{\xi - \xi_c}{\xi_c}, \quad s_i = \frac{r_i}{k_c^2 \xi_c \tilde{\Phi}_1},$$

with $i = 1, 2$.

Proof. See Appendix A.4

The existence and stability results relevant to the emergence of different spatial patterns are given by the following theorem.

Theorem 1. *The system (33) admits the following stationary states that correspond to the different spatial patterns:*

- i) homogeneous solution with $\rho_1 = \rho_2 = 0$; in this case, no pattern emerges;*
- ii) equilibria $\mathcal{S}_1 = (\bar{\rho}, 0)$ and $\mathcal{S}_2 = (0, \bar{\rho})$, with $\bar{\rho} = \sqrt{-\xi_m/s_1}$, corresponding to striped pattern, that exists for $s_1 < 0$ and are stable for $s_0 > 0$ and $s_2 < s_1 < 0$;*
- iii) equilibrium $\mathcal{Q} = (\tilde{\rho}, \tilde{\rho})$, with $\tilde{\rho} = \sqrt{-\xi_m/(s_1 + s_2)}$, corresponding to squared pattern, that exists for $s_1 < -s_2$ and is stable for $s_0 > 0$ and $s_1 < -|s_2|$.*

Proof. The conditions for the existence of both striped and squared patterns are directly provided by observing that $\xi_m > 0$ from (11). In order to inquire about the stability of patterns, let us compute the Jacobian matrix of the system (33) evaluated at the equilibria. For \mathcal{S}_1 we have

$$\mathcal{J}|_{\mathcal{S}_1} = \begin{pmatrix} -\frac{2\xi_m}{s_0} & 0 \\ 0 & \frac{(s_1 - s_2)\xi_m}{s_0 s_1} \end{pmatrix},$$

having trace and determinant

$$Tr \mathcal{J}|_{\mathcal{S}_1} = -\frac{(s_1 + s_2)\xi_m}{s_0 s_1}, \quad Det \mathcal{J}|_{\mathcal{S}_1} = \frac{2(-s_1 + s_2)\xi_m^2}{s_0^2 s_1}.$$

It is easy to check that $Tr \mathcal{J}|_{\mathcal{S}_1} = Tr \mathcal{J}|_{\mathcal{S}_2}$ and $Det \mathcal{J}|_{\mathcal{S}_1} = Det \mathcal{J}|_{\mathcal{S}_2}$. Then, the conditions for local asymptotic stability of the striped pattern providing $Tr \mathcal{J}|_{\mathcal{S}_1} < 0$ and $Det \mathcal{J}|_{\mathcal{S}_1} > 0$ are

$$s_0 > 0, \quad s_2 < s_1 < 0. \quad (34)$$

For the stability of the squared pattern, instead, we compute the Jacobian matrix evaluated at the equilibrium \mathcal{Q} , obtaining

$$\mathcal{J}|_{\mathcal{Q}} = -\frac{2\xi_m}{s_0(s_1+s_2)} \begin{pmatrix} s_1 & s_2 \\ s_2 & s_1 \end{pmatrix},$$

whose trace and determinant are

$$\text{Tr } \mathcal{J}|_{\mathcal{Q}} = -\frac{4s_1\xi_m}{s_0(s_1+s_2)}, \quad \text{Det } \mathcal{J}|_{\mathcal{Q}} = \frac{4(s_1-s_2)\xi_m^2}{s_0^2(s_1+s_2)}.$$

In this case, the conditions for local asymptotic stability of the squared pattern are

$$s_0 > 0, \quad s_1 < -|s_2|. \quad (35)$$

□

□

Remark 1. *The spatial patterns predicted by Theorem 1 correspond to structured distributions of demyelinated regions that may resemble histopathological observations in Multiple Sclerosis. Specifically, striped or band-like configurations can be interpreted as elongated plaques often seen along white-matter tracts, where demyelinated areas follow the orientation of deep medullary veins or fiber bundles, a pattern classically exemplified by “Dawson’s fingers” [28]; additionally, evidence from [33] shows elongated plaques even in lesions confined to the cortex. Some of these striped patterns may also represent individual segments of the concentric rings seen in Baló’s lesions [35], while squared or spotted arrangements reflect focal or concentric demyelinating areas reminiscent of either intracortical lesions [33] or the fully developed rings characteristic of Baló’s sclerosis [38].*

4 Numerical simulations

In this section, we numerically investigate the different possible behaviors of the reaction-diffusion system (3) by varying the parameter settings. The aim is to get patterning results in accordance with the theoretical findings outlined in the previous section. First of all, we fix the following parameter values:

$$\beta = 1, \quad \tau = 5, \quad \theta = 1, \quad \Omega = 1, \quad \zeta = 0.2. \quad (36)$$

Then, we analyze the dynamics of the model for different choices of the squeezing exponent γ , defining functions (2). In particular, we take $\gamma = 1, 2$, and we investigate the values for the parameters \mathcal{R} (given in (7)) and δ which determine the existence and stability of patterns in the two cases. The corresponding results are reported in Figure 1.

Remark 2. We point out here that the values for parameters relevant to cytokine dynamics and chemotactic motion are taken accordingly to the ones used in other mathematical models for Multiple Sclerosis, e.g. [23], and are biologically plausible. Conversely, the parameter values governing the progression of myelin destruction and the range for \mathcal{R} are chosen strictly for illustrative purposes here, with the intention that more specific estimations will be addressed in future investigations.

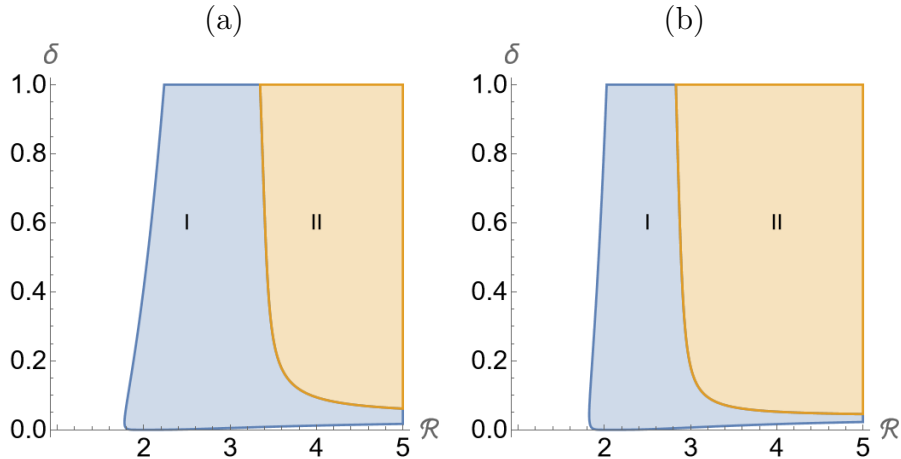


Figure 1: Values for \mathcal{R} and δ satisfying condition (34) (region I) or condition (35) (region II), taking values as in (36) and fixing $\gamma = 1$ in panel (a) and $\gamma = 2$ in panel (b).

In Figure 1, values for \mathcal{R} and δ leading to stable stripes as stated by condition (34) are in region I, while values providing stable squares stated by condition (35) are in region II, the two panels correspond to the cases $\gamma = 1$ (panel (a)) and $\gamma = 2$ (panel (b)).

Then, we depict the behavior of quantities involved in system (3)-(8). We take as reference case the one with $\gamma = 1$, $\delta = 0.6$ and $\mathcal{R} = 3.2$. From Figure 1, we observe that the stability of striped patterns is expected. Additionally, we take $\xi_m = 0.01$ that, with this choice of parameters, provides a value for the chemotactic sensitivity $\xi \simeq 13.31$. We perform numerical simulations using the software `VisualPDE` [41] in a square domain of size $L = 5\pi$. The results are shown in Figure 2, where the portion of myelin destroyed is reported.

As a second case, we keep the same values of parameters as before, except for $\gamma = 2$, providing a value for the chemotactic sensitivity $\xi \simeq 10.88$. In this case, as observable in Figure 1 again, a squared symmetry of the pattern is the stable configuration. The results are shown in Figure 3, where we observe a spotted spatial configuration. Indeed, in terms of modeling, a higher squeezing exponent leads to a higher diffusive term and a lower chemotactic term for self-reactive immune cells, which means that the random movement of cells is prevalent.

As a further test, we take the same parameters as the reference one, but we increase the parameter $\xi_m = 0.1$; in this way, the chemotactic sensitivity results $\xi \simeq 14.5$. The obtained configuration, as shown in Figure 4, is still striped one. The observable difference is in the

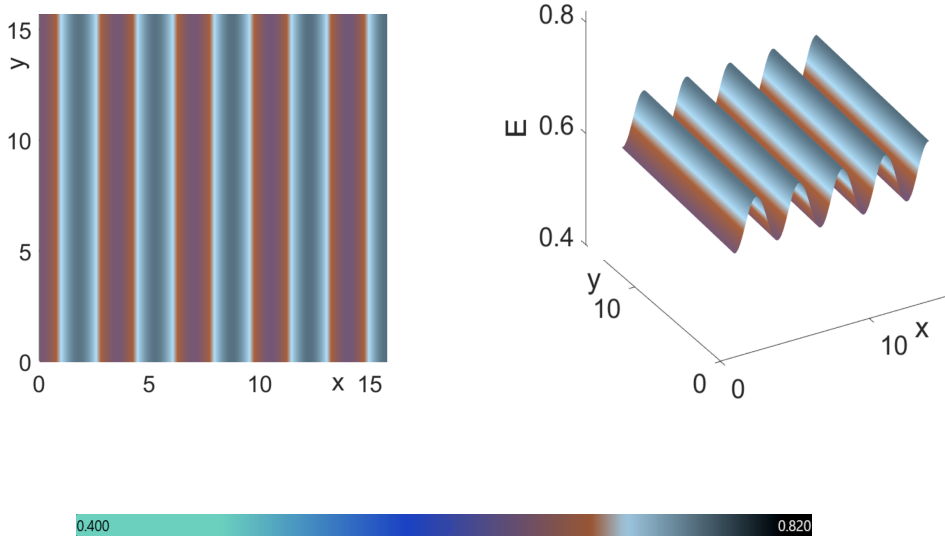


Figure 2: Long-time patterning of destroyed myelin portion (E), described by system (3), taking parameters $\gamma = 1$, $\delta = 0.6$ and $\mathcal{R} = 3.2$, $\xi = 13.31$.

minimum and maximum levels of consumed myelin, which in this case are, respectively, lower and higher w.r.t. the reference case. This is a consequence of the fact that the motion of self-reactive immune cells is majorly driven by the chemotactic attraction of cytokines, causing an inflammation, and consequently a myelin injury, more concentrated in some areas of the domain.

We point out that the patterns depicted above have been obtained by starting from a perturbation of the equilibrium resembling the results given in Subsection 3.2. Nevertheless, we underline that a weakly nonlinear analysis can be performed by decomposing the solution around the critical bifurcation value into three active dominant pairs of eigenmodes (i.e., as in the expression (13), with $m = 3$), as already proposed for other models describing Multiple Sclerosis (see, e.g., [5]). In this case, the solution is shaped by the combination of three amplitudes ρ_1, ρ_2, ρ_3 that can lead to the emergence of striped ($\rho_1 \neq 0, \rho_2 = \rho_3 = 0$), hexagonal ($\rho_1 = \rho_2 = \rho_3 \neq 0$) or rectangular ($0 \neq \rho_1 = \rho_2 \neq \rho_3 \neq 0$) patterns. Leaving this kind of analysis as a future step, we also perform numerical simulations for our model by starting from a random perturbation of the equilibrium. In particular, we take parameters' values $\gamma = 1$, $\delta = 0.6$, $\mathcal{R} = 3.2$, and perform a test by taking $\xi = 13.31$ (as in the reference case) and another taking $\xi = 14.5$ (as in the third case considered). The results obtained are reported in Figure 5 and show the coexistence of other stable spatial configurations, which show rectangular (panel (a)) or hexagonal (panel (b)) symmetry.

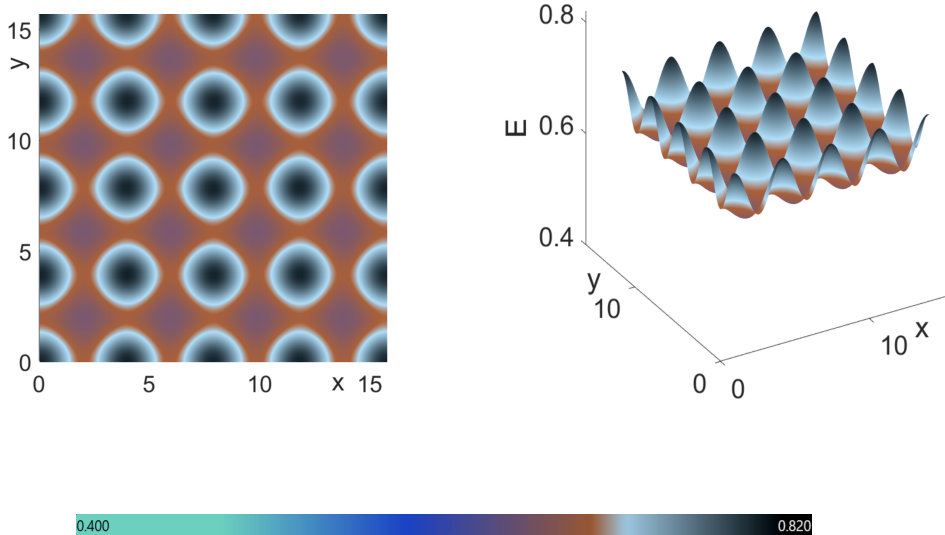


Figure 3: Long-time patterning of destroyed myelin portion (E), described by system (3), taking parameters $\gamma = 2$, $\delta = 0.6$ and $\mathcal{R} = 3.2$, $\xi = 10.88$.

5 Conclusions

In this study, we consider a reaction-diffusion model for Multiple Sclerosis and investigate the formation of two-dimensional spatial patterns that may replicate the development of demyelinating lesions in the white matter caused by the disease.

To describe the dynamics of self-reactive immune cells, cytokines, and the destroyed portion of myelin, we perform a reduction of the system introduced in paper [31]. We conduct a Turing instability analysis to determine parameter conditions that allow for the formation of spatial patterns. Subsequently, we carry out a weakly nonlinear analysis of the problem to further explore different patterning outcomes near the bifurcation value. Specifically, we decompose the solution in terms of two pairs of dominant eigenmodes.

We then identify the conditions that may lead to the emergence of striped or squared-like patterns and analyze their stability over time. The results obtained are numerically validated, revealing that different choices of the squeezing probability, which regulates the motion of immune cells in space, can lead to different pattern shapes. Furthermore, we observe that a higher value of the chemotactic parameter results in myelin damage more concentrated in specific regions of the domain.

Finally, we perform numerical simulations starting from random initial conditions, which lead to the formation of patterns exhibiting hexagonal or rectangular symmetry. A

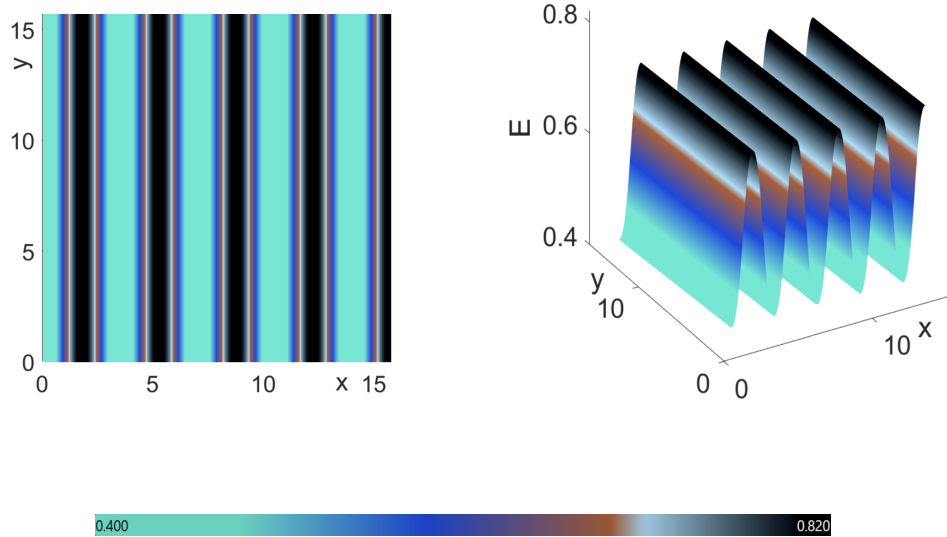


Figure 4: Long-time patterning of destroyed myelin portion (E), described by system (3), taking parameters $\gamma = 2$, $\delta = 0.6$ and $\mathcal{R} = 3.2$, $\xi = 14.5$.

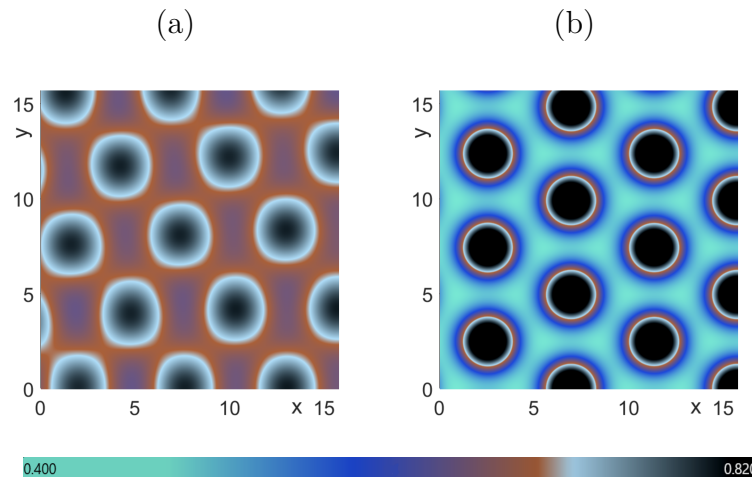


Figure 5: Long-time patterning of destroyed myelin portion (E), described by system (3) starting from a random perturbation of equilibrium, with parameters $\gamma = 1$, $\delta = 0.6$ and $\mathcal{R} = 3.2$. Panel (a): $\xi = 13.31$. Panel (b): $\xi = 14.5$.

novel contribution of this work is that, through a combination of weakly nonlinear analysis and numerical simulations, we demonstrate how key parameters, including the squeez-

ing probability and chemotactic sensitivity, can generate these two-dimensional patterns, providing a direct mechanistic explanation for the emergence of diverse lesion morphologies. These insights allow a better understanding of atypical lesion formation in Multiple Sclerosis, capturing features that cannot be reproduced by one-dimensional models or by approaches relying solely on oligodendrocyte loss.

These findings highlight the need for further analysis in future works, particularly considering the number of dominant eigenmodes larger than two. In addition, a wavefront invasion analysis of the problem could be performed to describe the spatio-temporal evolution of patterns.

Acknowledgments

We are thankful to the anonymous reviewers for their useful comments and suggestions. This work was performed in the framework of activities sponsored by the Italian National Group of Mathematical Physics (GNFM-INdAM) and by the University of Parma (Italy) and of Naples Federico II (Italy). RT is a post-doc fellow supported by the National Institute of Advanced Mathematics (INdAM), Italy. RDM and RT also thank the support of the University of Parma through the action Bando di Ateneo per la ricerca 2022, co-funded by MUR-Italian Ministry of Universities and Research - D.M. 737/2021 - PNR - PNRR - NextGenerationEU ‘Collective and self-organised dynamics: kinetic and network approaches’. The work was carried out in the frame of activities sponsored by the COST Action CA18232, by the Portuguese Projects UIDB/00013/2020 (<https://doi.org/10.54499/UIDB/00013/2020>), UIDP/00013/2020 of CMAT-UM (<https://doi.org/10.54499/UIDP/00013/2020>), and by the Portuguese national funds (OE), through the Project FCT/MCTES PTDC/03091/2022, “Mathematical Modelling of Multi-scale Control Systems: applications to human diseases – CoSysM3” (<https://doi.org/10.54499/2022.03091.PTDC>).

A Proof of results in Subsection 3.2

A.1 Proof of Proposition 2

As stated above, we are interested in describing spatial configurations arising from two pairs of eigenvectors. For this reason, we look for a solution of (18) in the form

$$\begin{pmatrix} u_1 \\ v_1 \\ w_1 \end{pmatrix} = \sum_{j=1}^2 [\mathbf{B}_j(t) e^{i \mathbf{k}_j \cdot \mathbf{x}} + \overline{\mathbf{B}}_j(t) e^{-i \mathbf{k}_j \cdot \mathbf{x}}], \quad (37)$$

i.e., we express the solution in terms of two active dominant pairs of eigenmodes $(\mathbf{k}_j, -\mathbf{k}_j)$, $j = 1, 2$, individuating angles of $\pi/2$, with $|\mathbf{k}_j| = k_c$ [32, 40]. Being (37) solution of (18),

we have

$$0 = \mathcal{L}_c \begin{pmatrix} u_1 \\ v_1 \\ w_1 \end{pmatrix} = (\mathbb{J} - k_c^2 \mathbb{D}_c) \begin{pmatrix} u_1 \\ v_1 \\ w_1 \end{pmatrix}.$$

As shown in Subsection 3.1, though, one has $\text{Det}(\mathbb{J} - k_c^2 \mathbb{D}_c) = 0$, and, since,

$$\mathbb{J} - k_c^2 \mathbb{D}_c = \begin{pmatrix} -1 - k_c^2 \tilde{\Phi}_0 & k_c^2 \xi_c \tilde{\Phi}_1 & 0 \\ \beta & -k_c^2 \delta - \tau & 0 \\ \frac{\zeta \theta (1 + 2\Omega)}{(1 + \Omega)(\zeta + \theta + \zeta \Omega)} & 0 & -\frac{\zeta + \theta + \zeta \Omega}{1 + \Omega} \end{pmatrix},$$

we can observe that the last two rows of the matrix are linearly independent, thus the kernel of $\mathbb{J} - k_c^2 \mathbb{D}_c$ has dimension 1. Consequently, the solution (37) is of the form

$$\begin{pmatrix} u_1 \\ v_1 \\ w_1 \end{pmatrix} = \begin{pmatrix} \rho_R \\ 1 \\ \rho_E \end{pmatrix} \sum_{j=1}^2 [\mathcal{W}_j(t) e^{i \mathbf{k}_j \cdot \mathbf{x}} + \overline{\mathcal{W}_j(t)} e^{-i \mathbf{k}_j \cdot \mathbf{x}}],$$

and, recalling the expression for k_c^2 in (12), the expressions for ρ_R and ρ_E read as in (22) and (23), respectively. This completes the proof. □

A.2 Proof of Proposition 3

First, we recast (19) as

$$\mathcal{L}_c \begin{pmatrix} u_2 \\ v_2 \\ w_2 \end{pmatrix} = \frac{\partial}{\partial T_1} \begin{pmatrix} u_1 \\ v_1 \\ w_1 \end{pmatrix} - \mathcal{H}_2 \left[\begin{pmatrix} u_1 \\ v_1 \\ w_1 \end{pmatrix} \right]. \quad (38)$$

We now exploit the Fredholm solvability condition, which ensures that, being B a Fredholm operator on a Banach (or Hilbert) space and b an element in the space, the inhomogeneous equation $Bx = b$ admits at least one solution if and only if b is orthogonal to every element in the kernel of the adjoint operator B^+ ; in other words, $Bx = b$ is solvable if and only if $\langle b, v \rangle = 0$ for all $v \in \ker(B^+)$. In this particular case, the operator \mathcal{L}_c may be interpreted as a linear continuous operator from the Banach space $\mathcal{Z} = (H^2(\Gamma_{\mathbf{x}}))^3$, generated by the functions $e^{i \tilde{\mathbf{k}} \cdot \mathbf{x}}$, $\tilde{\mathbf{k}} \in \mathbb{R}^2$, to $\mathcal{X} = (L^2(\Gamma_{\mathbf{x}}))^3$, with the inner product defined as the classical product in L^2 , see [9, 14] for the details. Consequently, the solvability condition states that, for a nontrivial solution to exist, the right-hand side of (38) must be orthogonal to

the kernel of the adjoint operator of \mathcal{L}_c , which we indicate by \mathcal{L}_c^+ and reads

$$\mathcal{L}_c^+ = \begin{pmatrix} -1 - \tilde{k}^2 \tilde{\Phi}_0 & \beta & 0 \\ \tilde{k}^2 \xi_c \tilde{\Phi}_1 & -\tilde{k}^2 \delta - \tau & \frac{\zeta \theta (1 + 2\Omega)}{(1 + \Omega)(\zeta + \theta + \zeta \Omega)} \\ 0 & 0 & -\frac{\zeta + \theta + \zeta \Omega}{1 + \Omega} \end{pmatrix},$$

being $\tilde{k} = |\tilde{\mathbf{k}}|$, and whose kernel is spanned by

$$\begin{pmatrix} 1 \\ \sigma_C \\ 0 \end{pmatrix} e^{i\mathbf{k}\cdot\mathbf{x}} + \text{c.c.}, \quad |\mathbf{k}| = k_c, \quad \sigma_C = \frac{1}{\beta} \left(1 + \sqrt{\frac{\tau \Phi_0}{\delta}} \right). \quad (39)$$

At this point, we substitute (21) into the right-hand side of (38), which results in a linear combination of terms e^0 , $e^{i\mathbf{k}_j\cdot\mathbf{x}}$, $e^{2i\mathbf{k}_j\cdot\mathbf{x}}$, $e^{i(\mathbf{k}_j - \mathbf{k}_i)\cdot\mathbf{x}}$. By isolating the coefficients corresponding to $e^{i\mathbf{k}_j\cdot\mathbf{x}}$, they write, for $j = 1, 2$,

$$\begin{pmatrix} R_u^j \\ R_v^j \\ R_w^j \end{pmatrix} = \begin{pmatrix} \rho_R \\ 1 \\ \rho_E \end{pmatrix} \frac{\partial \mathcal{W}_j}{\partial T_1} - \begin{pmatrix} \xi_1 \tilde{\Phi}_1 k_c^2 \mathcal{W}_j \\ 0 \\ 0 \end{pmatrix}. \quad (40)$$

The solvability condition implies the terms $(R_u^j, R_v^j, R_w^j)^T e^{i\mathbf{k}_j\cdot\mathbf{x}}$ to be orthogonal to (39) and thus

$$\left\langle \begin{pmatrix} R_u^j \\ R_v^j \\ R_w^j \end{pmatrix}, \begin{pmatrix} 1 \\ \sigma_C \\ 0 \end{pmatrix} \right\rangle = 0, \quad \text{for } j = 1, 2.$$

Consequently, by looking at (40), we obtain (24).

Successively, we have that the complete expression on the right-hand side of (38) results

$$\begin{aligned} & \begin{pmatrix} 2\rho_R^2 \\ 0 \\ \Psi_0 \end{pmatrix} (|\mathcal{W}_1|^2 + |\mathcal{W}_2|^2) + \sum_{j=1}^2 \begin{pmatrix} R_u^j \\ R_v^j \\ R_w^j \end{pmatrix} e^{i\mathbf{k}_j\cdot\mathbf{x}} \\ & + \begin{pmatrix} 2\rho_R \left(\rho_R + k_c^2 \left(\rho_R \tilde{\Phi}'_0 - \xi_c \rho_c \tilde{\Phi}'_1 \right) \right) \\ 0 \\ \Psi_1 \end{pmatrix} \\ & \times [\mathcal{W}_1 \mathcal{W}_2 e^{i(\mathbf{k}_1 + \mathbf{k}_2)\cdot\mathbf{x}} + \mathcal{W}_1 \overline{\mathcal{W}_2} e^{i(\mathbf{k}_1 - \mathbf{k}_2)\cdot\mathbf{x}}] \\ & + \sum_{j=1}^2 \begin{pmatrix} \rho_R^2 + 2k_c^2 \left(\rho_R^2 \tilde{\Phi}'_0 - \xi_c \rho_R \tilde{\Phi}'_1 \right) \\ 0 \\ \Psi_2 \end{pmatrix} \mathcal{W}_j^2 e^{2i\mathbf{k}_j\cdot\mathbf{x}} + \text{c.c.}, \end{aligned}$$

with

$$\begin{aligned}\Psi_0 &= \frac{4\theta\rho_R}{(1+\Omega)^2} \left(\rho_E(1+2\Omega) + \rho_R \left(1 + \frac{\theta}{\zeta} - \Omega - \frac{(\zeta+\theta)^2}{\zeta(\theta+\zeta(1+\Omega))} \right) \right), \\ \Psi_1 &= \frac{4\Theta\rho_R}{(1+\Omega)^2} \left(\rho_E(1+2\Omega) - \frac{\zeta\rho_R\Omega^2}{\Theta+\zeta(1+\Omega)} \right), \\ \Psi_2 &= \frac{2\theta\rho_R}{(1+\Omega)^2} \left(\rho_E(1+2\Omega) - \frac{\zeta\rho_R\Omega^2}{\theta+\zeta(1+\Omega)} \right).\end{aligned}$$

At this point, we claim that the solution $(u_2, v_2, w_2)^T$ for the non-homogeneous problem (38) has to be in the form

$$\begin{aligned}\begin{pmatrix} u_2 \\ v_2 \\ w_2 \end{pmatrix} &= \begin{pmatrix} X_0 \\ Y_0 \\ Z_0 \end{pmatrix} (|\mathcal{W}_1|^2 + |\mathcal{W}_2|^2) \\ &+ \sum_{j=1}^2 \left[\begin{pmatrix} \rho_R \\ 1 \\ \rho_E \end{pmatrix} \mathcal{V}_j + \mathcal{L}c^{-1} \begin{pmatrix} R_U^j \\ R_V^j \\ R_W^j \end{pmatrix} \mathcal{W}_j \right] e^{i\mathbf{k}_j \cdot \mathbf{x}} \\ &+ \begin{pmatrix} X_1 \\ Y_1 \\ Z_1 \end{pmatrix} [\mathcal{W}_1 \mathcal{W}_2 e^{i(\mathbf{k}_1 + \mathbf{k}_2) \cdot \mathbf{x}} + \mathcal{W}_1 \overline{\mathcal{W}_2} e^{i(\mathbf{k}_1 - \mathbf{k}_2) \cdot \mathbf{x}}] \\ &+ \sum_{j=1}^2 \begin{pmatrix} X_2 \\ Y_2 \\ Z_2 \end{pmatrix} \mathcal{W}_j^2 e^{2i\mathbf{k}_j \cdot \mathbf{x}} + \text{c.c.}.\end{aligned}$$

Then, the left-hand side of (38) reads

$$\begin{aligned}\mathcal{L}_c \begin{pmatrix} u_2 \\ v_2 \\ w_2 \end{pmatrix} &= \mathbb{J} \begin{pmatrix} X_0 \\ Y_0 \\ Z_0 \end{pmatrix} (|\mathcal{W}_1|^2 + |\mathcal{W}_2|^2) \\ &+ (\mathbb{J} - 2k_c^2 \mathbb{D}_c) \begin{pmatrix} X_1 \\ Y_1 \\ Z_1 \end{pmatrix} [\mathcal{W}_1 \mathcal{W}_2 e^{i(\mathbf{k}_1 + \mathbf{k}_2) \cdot \mathbf{x}} + \mathcal{W}_1 \overline{\mathcal{W}_2} e^{i(\mathbf{k}_1 - \mathbf{k}_2) \cdot \mathbf{x}}] \\ &+ (\mathbb{J} - 4k_c^2 \mathbb{D}_c) \sum_{j=1}^2 \begin{pmatrix} X_2 \\ Y_2 \\ Z_2 \end{pmatrix} \mathcal{W}_j^2 e^{2i\mathbf{k}_j \cdot \mathbf{x}} + \text{c.c.},\end{aligned}$$

where we have removed the inhomogeneous part in the $e^{i\mathbf{k}_j \cdot \mathbf{x}}$ -coefficient to avoid secular terms. To recover the solution of (38), then, we must solve the linear equations having as unknown the coefficients X_m, Y_m, Z_m , $m = 0, 1, 2$, given by

$$\begin{pmatrix} X_0 \\ Y_0 \\ Z_0 \end{pmatrix} = \mathbb{J}^{-1} \begin{pmatrix} 2\rho_R^2 \\ 0 \\ \Psi_0 \end{pmatrix},$$

$$\begin{pmatrix} X_1 \\ Y_1 \\ Z_1 \end{pmatrix} = (\mathbb{J} - 2k_c^2 \mathbb{D}_c)^{-1} \begin{pmatrix} 2\rho_R \left(\rho_R + k_c^2 \left(\rho_R \tilde{\Phi}'_0 - \xi_c \rho_c \tilde{\Phi}'_1 \right) \right) \\ 0 \\ \Psi_1 \end{pmatrix},$$

$$\begin{pmatrix} X_2 \\ Y_2 \\ Z_2 \end{pmatrix} = (\mathbb{J} - 4k_c^2 \mathbb{D}_c)^{-1} \begin{pmatrix} \rho_R^2 + 2k_c^2 \left(\rho_R^2 \tilde{\Phi}'_0 - \xi_c \rho_R \tilde{\Phi}'_1 \right) \\ 0 \\ \Psi_2 \end{pmatrix}.$$

The resolution of the three linear equations above provides the expressions for the coefficients given in (26)-(28), with

$$\Xi_0 = \frac{\zeta \theta (\zeta + 3\zeta \Omega + \theta (3 + 8\Omega))}{(\zeta + \theta + \zeta \Omega)^3},$$

$$\Xi_1 = \frac{2 \left(\sqrt{\delta} + 2\sqrt{\tau} \tilde{\Phi}_0 \right)}{\sqrt{\delta} \left(\sqrt{\delta} \tilde{\Phi}_0 (\tilde{\Phi}_1 - \tilde{\Phi}'_1) + \sqrt{\tau} (\tilde{\Phi}'_0 \tilde{\Phi}_1 - \tilde{\Phi}_0 \tilde{\Phi}'_1) \right) (\zeta + \theta + \zeta \Omega)^3}$$

$$\times \left[\sqrt{\tau} \left(\tilde{\Phi}'_0 \tilde{\Phi}_1 - \tilde{\Phi}_0 \tilde{\Phi}'_1 \right) (1 + \Omega) (\zeta + \theta + \zeta \Omega)^2 \right.$$

$$+ \sqrt{\delta} \tilde{\Phi}_0 \left(\theta^2 (\tilde{\Phi}_1 - \tilde{\Phi}'_1) (1 + \Omega) \right.$$

$$- 2\zeta \theta \left(\tilde{\Phi}'_1 (1 + \Omega)^2 + \tilde{\Phi}_1 (\theta + 3\theta \Omega - (1 + \Omega)^2) \right)$$

$$\left. \left. + \zeta^2 \left(\tilde{\Phi}_1 - \tilde{\Phi}'_1 (1 + \Omega)^3 + \tilde{\Phi}_1 \Omega (3 + \Omega (3 + 2\theta + \Omega)) \right) \right] \right],$$

$$\Xi_2 = \frac{-\zeta \theta \sqrt{\tau}}{\sqrt{\tilde{\Phi}_0} \left(-\sqrt{\delta} \tilde{\Phi}_0 (\tilde{\Phi}_1 - 2\tilde{\Phi}'_1) + 2\sqrt{\tau} \left(-\tilde{\Phi}'_0 \tilde{\Phi}_1 + \tilde{\Phi}_0 \tilde{\Phi}'_1 \right) \right) (\zeta + \theta + \zeta \Omega)^3}$$

$$\times \left[4\delta \sqrt{\tilde{\Phi}_0} (\tilde{\Phi}_1 - 2\tilde{\Phi}'_1) (1 + 2\Omega) (\zeta + \theta + \zeta \Omega) \right.$$

$$+ 2\tau \sqrt{\tilde{\Phi}_0} (\tilde{\Phi}'_0 \tilde{\Phi}_1 - \tilde{\Phi}_0 \tilde{\Phi}'_1) (1 + 2\Omega) (\zeta + \theta + \zeta \Omega)$$

$$+ \sqrt{\delta} \tau \left(8\theta \tilde{\Phi}'_0 \tilde{\Phi}_1 (1 + 2\Omega) + 8\zeta \tilde{\Phi}'_0 \tilde{\Phi}_1 (1 + \Omega) (1 + 2\Omega) \right.$$

$$+ \theta \tilde{\Phi}_0 \tilde{\Phi}_1 (19 + 56\Omega) - 10\theta \tilde{\Phi}_0 (\tilde{\Phi}'_1 + 2\tilde{\Phi}'_1 \Omega)$$

$$\left. \left. + \zeta \tilde{\Phi}_0 \left(\tilde{\Phi}_1 + \tilde{\Phi}_1 (3 - 16\Omega) \Omega - 10\tilde{\Phi}'_1 (1 + \Omega) (1 + 2\Omega) \right) \right] \right].$$

completing the proof. □

A.3 Proof of Proposition 4

We start by rewriting (20) as

$$\mathcal{L}_c \begin{pmatrix} u_3 \\ v_3 \\ w_3 \end{pmatrix} = \frac{\partial}{\partial T_1} \begin{pmatrix} u_2 \\ v_2 \\ w_2 \end{pmatrix} + \frac{\partial}{\partial T_2} \begin{pmatrix} u_1 \\ v_1 \\ w_1 \end{pmatrix} - \mathcal{H}_3 \left[\begin{pmatrix} u_1 \\ v_1 \\ w_1 \end{pmatrix}, \begin{pmatrix} u_2 \\ v_2 \\ w_2 \end{pmatrix} \right].$$

As done before, we rely on the Fredholm solvability condition. We substitute the expressions (21) and (25) in the right-hand term of (20), and isolate the (24), that results

$$\begin{pmatrix} S_u^j \\ S_v^j \\ S_w^j \end{pmatrix} = \begin{pmatrix} \rho_R \\ 1 \\ \rho_E \end{pmatrix} \left(\frac{\partial \mathcal{V}_j}{\partial T_1} + \frac{\partial \mathcal{W}_j}{\partial T_2} \right) - \begin{pmatrix} \tilde{\Phi}_1 k_c^2 (\xi_1 \mathcal{V}_j + \xi_2 \mathcal{W}_j) \\ 0 \\ 0 \end{pmatrix} \\ + \left[\begin{pmatrix} -r_1 \\ 0 \\ t_1 \end{pmatrix} |\mathcal{W}_j|^2 + \begin{pmatrix} -r_2 \\ 0 \\ t_2 \end{pmatrix} |\mathcal{W}_l|^2 \right] \mathcal{W}_j,$$

for $j, l = 1, 2, j \neq l$, with coefficients r_1 and r_2 given in (30) and

$$\begin{aligned} t_1 &= q_1 (q_2 + (Z_0 + Z_2) q_3 + (X_0 + X_2) q_4), \\ t_2 &= q_1 (2 q_2 + (Z_0 + 2 Z_1) q_3 + (X_0 + 2 X_1) q_4), \\ q_1 &= \frac{2 \theta \rho_R}{(1 + \Omega)^3 (\zeta + \theta + \zeta \Omega)^2}, \quad q_2 = 9 \zeta \rho_R^2 \Omega^2 (\zeta + \theta + \zeta \Omega), \\ q_3 &= (1 + \Omega) (1 + 2 \Omega) (\theta + \zeta (1 + \Omega))^2, \\ q_4 &= \zeta (1 + \Omega) (\theta - 2 \zeta \Omega^2 (1 + \Omega) + 2 \theta \Omega (2 + \Omega)). \end{aligned}$$

At this point, imposing

$$\left\langle \begin{pmatrix} S_u^j \\ S_v^j \\ S_w^j \end{pmatrix}, \begin{pmatrix} 1 \\ \sigma_C \\ 0 \end{pmatrix} \right\rangle = 0, \quad \text{for } j = 1, 2,$$

with σ_C defined in (39), we find the relation (29), completing the proof. □

A.4 Proof of Proposition 5

First, equations (24) - (29) allow us to rewrite (32), for $j, l = 1, 2, l \neq j$, as

$$\begin{aligned} (\rho_R + \sigma_C) \frac{dA_j}{dt} &= k_c^2 \tilde{\Phi}_1 (\mathcal{W}_j (\eta^2 \xi_1 + \eta^3 \xi_2) + \eta^3 \xi_1 \mathcal{V}_j) \\ &\quad + \eta^3 (r_1 |\mathcal{W}_j|^2 + r_2 |\mathcal{W}_l|^2) \mathcal{W}_j, \end{aligned}$$

omitting the higher-order terms.

From (15) we may write, still omitting higher-order terms,

$$\eta \xi_1 = \xi - \xi_c - \eta^2 \xi_2,$$

obtaining

$$\begin{aligned} (\rho_R + \sigma_C) \frac{dA_j}{dt} = & k_c^2 \tilde{\Phi}_1 (\xi - \xi_c) (\eta \mathcal{W}_j + \eta^2 \xi_1 \mathcal{V}_j) \\ & + \eta^3 (r_1 |\mathcal{W}_j|^2 + r_2 |\mathcal{W}_l|^2) \mathcal{W}_j, \end{aligned}$$

which, from (31), becomes

$$s_0 \frac{dA_j}{dt} = \xi_m A_j + A_j (s_1 |A_j|^2 + s_2 |A_l|^2), \quad (41)$$

where

$$s_0 = \frac{\rho_R + \sigma_C}{k_c^2 \xi_c \tilde{\Phi}_1}, \quad \xi_m = \frac{\xi - \xi_c}{\xi_c}, \quad s_i = \frac{r_i}{k_c^2 \xi_c \tilde{\Phi}_1},$$

with $i = 1, 2$.

By decomposing each amplitude into modulus and phase angle as

$$A_j = \rho_j e^{i\phi_j},$$

and splitting the real and imaginary parts of equations (41), we get the system:

$$\begin{aligned} s_0 \left(\rho_1 \frac{d\phi_1}{dt} \cos \phi_1 + \frac{d\rho_1}{dt} \sin \phi_1 \right) &= \rho_1 (\xi_m + s_1 \rho_1^2 + s_2 \rho_2^2) \sin \phi_1, \\ s_0 \left(\rho_2 \frac{d\phi_2}{dt} \cos \phi_2 + \frac{d\rho_2}{dt} \sin \phi_2 \right) &= \rho_2 (\xi_m + s_1 \rho_2^2 + s_2 \rho_1^2) \sin \phi_2, \\ s_0 \left(\frac{d\rho_1}{dt} \cos \phi_1 - \rho_1 \frac{d\phi_1}{dt} \sin \phi_1 \right) &= \rho_1 (\xi_m + s_1 \rho_1^2 + s_2 \rho_2^2) \cos \phi_1, \\ s_0 \left(\frac{d\rho_2}{dt} \cos \phi_2 - \rho_2 \frac{d\phi_2}{dt} \sin \phi_2 \right) &= \rho_2 (\xi_m + s_1 \rho_2^2 + s_2 \rho_1^2) \cos \phi_2, \end{aligned}$$

that provides

$$\begin{aligned} \frac{d\phi_1}{dt} &= 0 \\ \frac{d\phi_2}{dt} &= 0 \\ s_0 \frac{d\rho_1}{dt} &= \xi_m \rho_1 + s_1 \rho_1^3 + s_2 \rho_2^2 \rho_1 \\ s_0 \frac{d\rho_2}{dt} &= \xi_m \rho_2 + s_1 \rho_2^3 + s_2 \rho_1^2 \rho_2, \end{aligned}$$

completing the proof. □

References

- [1] R. Amoriello, C. Memo, L. Ballerini, and C. Ballerini. The brain cytokine orchestra in multiple sclerosis: from neuroinflammation to synaptopathology. *Mol. Brain*, 17(1):4, 2024.
- [2] V. I. Arnold. *Ordinary Differential Equations*. Springer Science & Business Media, Berlin, Heidelberg, 1992.
- [3] R. Barresi, E. Bilotta, F. Gargano, M. C. Lombardo, P. Pantano, and M. Sammartino. Wavefront invasion for a chemotaxis model of multiple sclerosis. *Ric. Mat.*, 65:423–434, 2016.
- [4] M. Bisi, M. Groppi, G. Martalò, and C. Soresina. A chemotaxis reaction–diffusion model for Multiple Sclerosis with Allee effect. *Ric. Mat.*, 73(Suppl 1):29–46, 2024.
- [5] M. Bisi, M. Groppi, G. Martalò, and R. Travaglini. Derivation from kinetic theory and 2-D pattern analysis of chemotaxis models for Multiple Sclerosis. *J. Math. Biol.*, 91(43), 2025.
- [6] I. Bordi, R. Umeton, V. A. G. Ricigliano, V. Annibali, R. Mechelli, G. Ristori, F. Grassi, M. S., and A. Sutera. A mechanistic, stochastic model helps understand multiple sclerosis course and pathogenesis. *Int. J. Genom.*, 2013(1):910321, 2013.
- [7] V. Calvez and R. H. Khonsari. Mathematical description of concentric demyelination in the human brain: Self-organization models, from liesegang rings to chemotaxis. *Math. Comput. Model.*, 47(7-8):726–742, 2008.
- [8] M. F. P. Costa, M. P. Ramos, C. Ribeiro, and A. J. Soares. Optimal control model of immunotherapy for autoimmune diseases. *Math. Meth. Appl. Sci.*, 44(11):8883–8902, 2021.
- [9] G. Da Prato and J. Zabczyk. *Second Order Partial Differential Equations in Hilbert Spaces*, volume 293. Cambridge University Press, Cambridge, 2002.
- [10] N. A. Danke, D. M. Koelle, C. Yee, S. Beheray, and W. W. Kwok. Autoreactive T cells in healthy individuals. *J. Immunol.*, 172(10):5967–5972, 2004.
- [11] M. Delitala, U. Dianzani, T. Lorenzi, and M. Melensi. A mathematical model for immune and autoimmune response mediated by T-cells. *Comput. Math. Appl.*, 66(6):1010–1023, 2013.
- [12] R. Della Marca, M. P. Machado Ramos, C. Ribeiro, and A. J. Soares. Mathematical modelling of oscillating patterns for chronic autoimmune diseases. *Math. Meth. Appl. Sci.*, 45(11):7144–7161, 2022.

- [13] F. Frascaoli, I. Roos, C. B. Malpas, and T. Kalincik. The dynamics of relapses during treatment switch in relapsing-remitting multiple sclerosis. *J. Theor. Biol.*, 541:111091, 2022.
- [14] M. Haragus and G. Iooss. *Local Bifurcations, Center Manifolds, and Normal Forms in Infinite-Dimensional Dynamical Systems*. Springer Science & Business Media, London, 2010.
- [15] R. A. Høglund, T. Holmøy, H. F. Harbo, and A. A. Maghazachi. A one year follow-up study of natural killer and dendritic cells activities in multiple sclerosis patients receiving glatiramer acetate (GA). *PLoS One*, 8(4):e62237, 2013.
- [16] R. Hoyle. *Pattern Formation. An Introduction to Methods*. Cambridge University Press, Cambridge, 2006.
- [17] E. Kamma, W. Lasisi, C. Libner, H. S. Ng, and J. R. Plemel. Central nervous system macrophages in progressive multiple sclerosis: relationship to neurodegeneration and therapeutics. *J. Neuroinflammation*, 19(1):45, 2022.
- [18] R. H. Khonsari and V. Calvez. The origins of concentric demyelination: self-organization in the human brain. *PLoS One*, 2(1):e150, 2007.
- [19] M. Kolev and I. Nikolova. A mathematical model of some viral-induced autoimmune diseases. *Math. Applicanda*, 46(1), 2018.
- [20] H. Lassmann. Multiple sclerosis pathology: evolution of pathogenetic concepts. *Brain Pathol.*, 15(3):217–222, 2005.
- [21] H. Lassmann, W. Brück, and C. F. Lucchinetti. The immunopathology of multiple sclerosis: an overview. *Brain Pathol.*, 17(2):210–218, 2007.
- [22] H. Lassmann, J. Van Horssen, and D. Mahad. Progressive multiple sclerosis: pathology and pathogenesis. *Nat. Rev. Neurol.*, 8(11):647–656, 2012.
- [23] M. Lombardo, R. Barresi, E. Bilotta, F. Gargano, P. Pantano, and M. Sammartino. Demyelination patterns in a mathematical model of multiple sclerosis. *J. Math. Biol.*, 75:373–417, 2017.
- [24] M. P. Machado Ramos, C. Ribeiro, and A. J. Soares. A kinetic model of T cell autoreactivity in autoimmune diseases. *J. Math. Biol.*, 79(6-7):2005–2031, 2019.
- [25] D. H. Mahad, B. D. Trapp, and H. Lassmann. Pathological mechanisms in progressive multiple sclerosis. *Lancet Neurol.*, 14(2):183–193, 2015.
- [26] M. Menale and R. Travaglini. A nonconservative kinetic model under the action of an external force field for modeling the medical treatment of autoimmune response. *Commun. Nonlinear Sci. Numer. Simul.*, 128:108126, 2024.

- [27] M. Mimpen, J. Smolders, R. Hupperts, and J. Damoiseaux. Natural killer cells in multiple sclerosis: a review. *Immunol. Lett.*, 222:1–11, 2020.
- [28] R. A. Multz, P. Jamshidi, and J. T. Ahrendsen. Multiple sclerosis: a practical review for pathologists. *J. Pathol. Transl. Med.*, 2025.
- [29] J. Murray. *Mathematical Biology II: Spatial Models and Biomedical Applications*, volume 18 of *Interdisciplinary Applied Mathematics*. Springer, New York, 3rd edition, 2003.
- [30] J. M. Oliveira, A. J. Soares, and R. Travaglini. Kinetic models leading to pattern formation in the response of the immune system. *Rivista di Matematica della Università di Parma*, 15(1):185–212, 2024.
- [31] J. M. Oliveira and R. Travaglini. Reaction–diffusion systems derived from kinetic theory for Multiple Sclerosis. *Math. Models Methods Appl. Sci.*, 34(07):1279–1308, 2024.
- [32] Q. Ouyang. *Pattern Formation in Reaction–Diffusion Systems*. Shanghai Scientific and Technological Education Publishing House, Shanghai, 2000.
- [33] J. W. Peterson, L. Bö, S. Mörk, A. Chang, and B. D. Trapp. Transected neurites, apoptotic neurons, and reduced inflammation in cortical multiple sclerosis lesions. *Ann. Neurol.*, 50(3):389–400, 2001.
- [34] C. Selmi, B. Gao, and M. E. Gershwin. The long and latent road to autoimmunity. *Cell. Mol. Immunol.*, 15(6):543–546, 2018.
- [35] C. Stadelmann, S. Ludwin, T. Tabira, A. Guseo, C. F. Lucchinetti, L. Leel-Össy, A. T. Ordinario, W. Brück, and H. Lassmann. Tissue preconditioning may explain concentric lesions in Baló’s type of multiple sclerosis. *Brain*, 128(5):979–987, 2005.
- [36] R. Travaglini. A reaction-diffusion model for relapsing-remitting multiple sclerosis with a treatment term. In *Numerical Mathematics and Advanced Applications ENUMATH 2023*, 2023. In press.
- [37] A. M. Turing. The chemical basis of morphogenesis. *Phil. Trans. R. Soc. Lond. B*, 237:37–72, 1952.
- [38] D. Tzanetakos, A. G. Vakrakou, J. S. Tzartos, G. Velonakis, M. E. Evangelopoulos, M. Anagnostouli, G. Koutsis, E. Dardiotis, E. Karavasilis, P. Toulas, L. Stefanis, and C. Kilidireas. Heterogeneity of Baló’s concentric sclerosis: a study of eight cases with different therapeutic concepts. *BMC Neurol.*, 20(1):400, 2020.
- [39] M. van Hecke, P. Hohenberg, and W. van Saarloos. Amplitude equations for pattern forming systems. In H. van Beijeren and M. Ernst, editors, *Fundamental Problems in Statistical Mechanics VIII*, pages 245–278. North-Holland, Amsterdam, 1994.

- [40] D. Walgraef. *Spatio-Temporal Pattern Formation: with Examples from Physics, Chemistry, and Materials Science*. Springer Science & Business Media, New York, 2012.
- [41] B. J. Walker, A. K. Townsend, A. K. Chudasama, and A. L. Krause. VisualPDE: rapid interactive simulations of partial differential equations. *Bull. Math. Biol.*, 85(11):113, 2023.
- [42] Z. Wang and T. Hillen. Classical solutions and pattern formation for a volume filling chemotaxis model. *Chaos*, 17(3):037108, 2007.
- [43] WHO - World Health Organization. Multiple sclerosis, 2023. (Accessed on November 2025).
- [44] A. L. Zozulya and H. Wiendl. The role of regulatory T cells in multiple sclerosis. *Nat. Clin. Pract. Neurol.*, 4(7):384–398, 2008.